Research Square

Preprints are preliminary reports that have not undergone peer review.
They should not be considered conclusive, used to inform clinical practice,
or referenced by the media as validated information.

Investigating the divergence of β-lactamase PDC variants conferring various antibiotic resistance profiles in Pseudomonas aeruginosa, coupled with the molecular profiling of PDC-266

Hailong Lin

203004@wzhealth.com

The Second Affiliated Hospital and Yuying Children's Hospital, Wenzhou Medical University

Leting Huang

The Second Affiliated Hospital and Yuying Children's Hospital, Wenzhou Medical University

Kaichun Lin

The First People's Hospital of Yongkang

Lv Pan

The First People's Hospital of Yongkang

Jian Zhou

The First People's Hospital of Yongkang

Research Article

Keywords: Pseudomonas aeruginosa, β-lactamase, Meropenem, N131S, Antibiotic Resistance

Posted Date: July 8th, 2026

DOI: https://doi.org/10.21203/rs.3.rs-10024309/v1

License: This work is licensed under a Creative Commons Attribution 4.0 International License.
Read Full License

Additional Declarations:
No competing interests reported.

Tables are available in the Supplementary Files section.

Version of Record: A version of this preprint was published at BMC Microbiology on September 22nd, 2026. See the published version at https://doi.org/10.1186/s12866-026-05679-0.

Investigating the divergence of β-lactamase PDC variants conferring various antibiotic resistance profiles in *Pseudomonas aeruginosa*, coupled with the molecular profiling of PDC-266

Hailong Lin[1*], Leting Huang[2], Kaichun Lin[3**], Pan Lv[4], Jian Zhou[5]

[1] Department of Pediatrics, The Second Affiliated Hospital and Yuying Children's Hospital, Wenzhou Medical University, Wenzhou 325027, China

[2] Department of Hematology and Oncology, The Second Affiliated Hospital and Yuying Children's Hospital, Wenzhou Medical University, Wenzhou 325027, China

[3] Department of Otorhinolaryngology, The First People's Hospital of Yongkang, Jinhua, China

[4] Department of Clinical Laboratory, The First People's Hospital of Yongkang, Jinhua, China

[5] Department of Pediatrics, The First People's Hospital of Yongkang, Jinhua, China

*** Correspondence:** Hailong Lin, 203004@wzhealth.com, The Second Affiliated Hospital and Yuying Children's Hospital, Wenzhou Medical

University, Wenzhou 325027, zhejiang Province, China

** **Co-Correspondence:** Kaichun Lin, heidylkc@qq.com, The First People's Hospital of Yongkang, Jinhua, zhejiang Province, China

Running title: Molecular profiling of PDC-266

Abstract

Background: *Pseudomonas aeruginosa* is a critical pathogen in

hospital-acquired infections, with resistance primarily mediated by chromosomally encoded PDC genes. While wild-type PDCs typically hydrolyze penicillins and cephalosporins, mutations can expand their substrate spectrum. This study investigates the molecular epidemiology and biochemical characteristics of PDC variants, particularly PDC-266.

Methods: We sequenced the genomic DNA of 14 P. aeruginosa clinical isolates. Antimicrobial susceptibility testing was performed via agar dilution. The plasmids expressing blaPDC-3, blaPDC-5, blaPDC-10, and blaPDC-266 were transformed into *E. coli* DH5α. Site-directed mutagenesis (Q79R, N131S, L205V) was conducted to evaluate the impact of individual residues. Steady-state kinetic parameters and inhibition assays were determined for purified enzymes. Molecular docking was utilized to analyze the structural interaction between PDC variants and meropenem.

Results: Among the 14 isolates, four PDC variants were identified: PDC-3 (n=6), PDC-5 (n=5), PDC-10 (n=2), and PDC-266 (n=1). The PDC-266-producing isolate (PA1CSR) exhibited a significantly elevated MIC for meropenem (64 μg/mL). Transformation assays confirmed that PDC-266 conferred an 8-fold increase in Meropenem MIC compared to PDC-3, PDC-5, and PDC-10. Kinetic analysis revealed that PDC-266 and the engineered variant PDC-3-N131S possessed moderate catalytic efficiency against meropenem (kcat/Km: 15–16.5 $mM^{-1} \cdot s^{-1}$). Molecular

docking demonstrated that the N131S substitution alters the active site cavity, making it narrower and deeper, facilitating stronger hydrogen bonding between meropenem and the catalytic residue SER-64.

Conclusion: This study characterizes PDC-266, a PDC variant capable of hydrolyzing Meropenem. The N131S substitution is identified as the critical determinant for this expanded substrate specificity by remodeling the active site architecture. Despite this expansion, PDC-266 remains susceptible to Avibactam and Sulbactam.

Keywords: *Pseudomonas aeruginosa*, β-lactamase, Meropenem, N131S, Antibiotic Resistance

Highlights

Discovery of PDC-266: Identification of a novel Pseudomonas-derived cephalosporinase variant in clinical P. aeruginosa isolates.

Expanded Substrate Spectrum: PDC-266 demonstrates unique carbapenemase-like activity, specifically hydrolyzing meropenem.

Key Mutation: The N131S substitution is the critical driver of meropenem resistance, increasing catalytic efficiency by 8-fold.

Structural Mechanism: N131S induces a conformational change, creating a narrower and deeper active site pocket that optimizes meropenem binding.

Introduction

Pseudomonas aeruginosa (*P. aeruginosa*) is the main pathogen of hospital-acquired infections, often causing infections in hospitalized or immunocompromised patients. It has been identified as the third leading cause of hospital-acquired infections (9.9%), ranking after *Clostridium difficile* and *Staphylococcus aureus*. Antibiotic-resistant *P. aeruginosa* has become a global public health issue(1). The mechanism of resistance involves multiple levels, among which enzymatic inactivation, such as the secretion of β-lactamases to hydrolyze antibiotics such as penicillins and cephalosporins, is an important method. PDCs (Pseudomonas-derived cephalosporinase) are a type of important β-lactamases. PDCs belong to the Ambler Class C serine enzymes (with one serine residue at the active site) and can hydrolyze β-lactam antibiotics. The bla_{PDC} gene is usually located on the chromosome of *P. aeruginosa*, rather than on the plasmid, which means that PDCs are part of the inherent resistance mechanism of this bacterium(2). PDCs have a wide range of substrate hydrolysis, mainly including penicillins and cephalosporins. For carbapenems such as imipenem and meropenem, PDCs have very weak hydrolytic ability and are generally not considered carbapenemases(3). However, due to their inducible nature and propensity for mutation leading to high-level expression, PDCs pose a significant risk for the escalation of antibiotic resistance(4).

Due to the widespread global use of antibiotics, the number of PDC

allelic variants is substantial and continues to grow. According to different databases such as BLDB, CARD, and NCBI, over 600 PDC variants have been discovered so far, and this number is still increasing(5).

Mutations in the regulatory network or within the structural ampC (PDC) gene itself can lead to significantly elevated and broadened resistance. Wild-type/basal-type strains (such as PDC-1, characterized by typical group 2e enzyme properties) can be induced and effectively inhibited by enzyme inhibitors (such as tazobactam); they mainly hydrolyze penicillins and early cephalosporins, with weak hydrolytic ability against fourth-generation cephalosporins (cefepime) and carbapenems(6). Extended-spectrum cephalosporinase (ESAC) variants represent the most critical mutant category. Through key site mutations (such as at the D223 site located in the Ω-loop, where Asp changes to Gly, Glu, Ala, etc.), these variants have gained enhanced hydrolytic ability, particularly against fourth-generation cephalosporins (cefepime). Strains carrying such variants are resistant to drugs such as cefepime, even if their expression levels are not high. They are still typically inhibited by enzyme inhibitors such as tazobactam(7,8). Enzyme inhibitor-resistant (IRT) variants have mutations that can directly interfere with the binding of enzyme inhibitors (such as tazobactam and clavulanic acid), resulting in decreased sensitivity to inhibitors. Mutations such as Y150H, A224T/V,

and P254S are common; these render combination formulations like piperacillin-tazobactam ineffective, thereby significantly limiting treatment options(9,10).

In this study, based on the sequencing of mixed genomic DNA from 88 human clinical *P. aeruginosa* isolates, we investigated the variants of PDC and the characteristics of the resistance gene-related sequences of the bacteria.

2 Materials and methods

2.1 Bacterial strains

A total of 88 clinical isolates of *P. aeruginosa* (hereinafter referred to as 'PA' within strain identifiers) were isolated from two regional hospitals in Zhejiang Province, China, between 2023 and 2024. Species identification was performed using the Vitek-60 automated microbial identification system (bioMérieux, Craponne, France) and confirmed via biochemical testing followed by 16S rRNA gene sequencing.

2.2 Antimicrobial Susceptibility Test

Susceptibility profiles were established via the agar dilution technique, with results interpreted in strict adherence to the 2024 guidelines issued by the Clinical and Laboratory Standards Institute (CLSI). *P. aeruginosa* ATCC 27853 served as the reference strain for quality assurance. We evaluated Susceptibility against a panel of thirteen agents using agar dilution: ampicillin (AMP), ampicillin/sulbactam (ASP),

piperacillin (PIP), piperacillin/tazobactam (TZP), aztreonam (AZT), ceftriaxone (CTX), ceftazidime (CAZ), cefepime (FEP), cefoperazone (CFPM), cefoperazone/sulbactam (CFPM/SUL), meropenem (MEM), and imipenem (IMP). Notably, resistance to the combination agent ceftazidime/avibactam (CAZ/AVI) was assessed through broth microdilution rather than agar dilution.

2.3 DNA Extraction and Sequencing

Individual isolates underwent overnight cultivation in 5 mL of Luria-Bertani (LB) medium at 37°C for 16 hours, followed by genomic DNA extraction utilizing the AxyPrep Bacterial Genomic DNA Miniprep kit (Axygen Scientific, Union City, CA, USA). For sequencing purposes, DNA was similarly harvested from single colonies grown on MacConkey agar under identical thermal and temporal conditions (37°C, 16 h) using the same extraction protocol. High-throughput sequencing was conducted by Personalbio Technology (Shanghai, China) employing both Illumina HiSeq 2500 and PacBio RS II platforms. Initial assembly of PacBio long-read data was performed using Canu (v1.6) to generate contiguous genomic sequences. Subsequently, paired-end FASTQ files derived from the Illumina HiSeq 2500 system were aligned against this primary assembly to validate and refine assembly accuracy. Potential open reading frames (ORFs) were identified via Glimmer software and functionally annotated against the UniProt/Wish Prot databases. Protein-coding gene

annotation relied on BLASTx searches against the non-redundant protein database, applying an e-value cutoff of 1e−5. Furthermore, genes associated with antimicrobial resistance and mobile genetic elements were characterized using default settings within specialized repositories, including ISfinder, INTEGRALL, and ResFinder.

2.4 Pulsed-Field Gel Electrophoresis

Pulsed-field gel electrophoresis (PFGE) was executed following the digestion of genomic DNA with 20 units of the *Spe I* restriction endonuclease (Takara, Dalian, China). Fragment separation was achieved using a CHEF-Mapper XA system (Bio-Rad, Hercules, CA, USA) over an 18-hour period at 6 V/cm and 14°C. The electrophoretic conditions included a 120° reorientation angle and pulse times ramping from 5 to 25 seconds. Separation occurred within 1% Seakem Gold agarose prepared with cell suspension buffer (comprising 10 mL of 1 M Tris–HCl [pH 8.0], 20 mL of 0.5 M EDTA [pH 8.0], and sterilized water to a final volume of 100 mL) and cell lysis buffer (containing 25 mL of 1 M Tris–HCl [pH 8.0], 50 mL of 0.5 M EDTA [pH 8.0], 50 mL of 10% Sarcosyl, adjusted to 100 mL with sterilized water). Phylogenetic relationships derived from PFGE profiles were elucidated via UPGMA clustering with a 2% tolerance threshold, wherein similarity cutoffs of 85% and 95% delineated distinct PFGE clusters.

2.5 Multilocus sequence typing

Multilocus sequence typing (MLST) of *P. aeruginosa* isolates isolates involved PCR amplification followed by sequencing of seven housekeeping genes, *gapA*, *infB*, *mdh*, *pgi*, *phoE*, *rpoB*, and *tonB*. Resulting sequences were queried against the Pasteur Institute MLST database (https://bigsdb.pasteur) to assign specific sequence types (STs), utilizing tools such as INTEGRALL and ResFinder for comprehensive analysis.

2.6 Plasmid transformation assays

To characterize the resistance phenotypes conferred by $bla_{\text{PDC-3}}$, $bla_{\text{PDC-5}}$, $bla_{\text{PDC-10}}$, $bla_{\text{KPC-266}}$ and $bla_{\text{OXA-50}}$, plasmid transformation assays were conducted. Target genes were amplified via PCR using specific primer pairs: $bla_{\text{PDC-3}}$ FF(BamHI) 5'-GGATCCGTCAGGAGGAGGATGCGACG-3' and $bla_{\text{PDC-3}}$ FR(HindIII) 5'-AAGCTTAAGCCTAGATTTTCCCCGCC-3'; $bla_{\text{PDC-5}}$ FF(BamHI) 5'-GGATCCGCGCTCATGGCACCATCATA-3' and $bla_{\text{PDC-5}}$ FR(HindIII) 5'-AAGCTTAAGCCTAGATTTTCCCCGCC-3'; $bla_{\text{PDC-10}}$ FF(BamHI) 5'-GGATCCCCAGGTCTTGAGCGACATCC-3' and $bla_{\text{PDC-10}}$ FR(HindIII) 5'-AAGCTTGAGTATTCGTCGTTTGCCGC-3'; $bla_{\text{PDC-266}}$ FF(BamHI) 5'-GGATCCCACCATCATAGCCAGGACCG-3' and $bla_{\text{PDC-266}}$ FR(HindIII) 5'-AAGCTTTCTCATGCAGCCAACGACAA-3'; $bla_{\text{OXA-50}}$ FF(BamHI) 5'-GGATCCCTACCCTTTCGTCGCCAAGT-3' and $bla_{\text{OXA-50}}$

FR(HindIII) 5’-AAGCTTTGTATGGCTATCACCTCGGC-3’. Amplified products were ligated into the pUCP24 vector and subsequently introduced into *Escherichia coli* (*E. coli*) DH5α competent cells via electroporation. Transformants were selected on Mueller–Hinton agar plates supplemented with ceftazidime (8 μg/mL). Successful gene acquisition in transformants was verified through PCR amplification and subsequent nucleotide sequencing..

Furthermore, an analogous strategy was implemented to isolate the full-length ORF of $bla_{\text{PDC-3}}$, $bla_{\text{PDC-5}}$, $bla_{\text{PDC-10}}$, $bla_{\text{KPC-266}}$ and $bla_{\text{OXA-50}}$ for subsequent insertion into the pET-28a vector. Specifically, PCR-amplified targets were ligated into the pET-28a backbone at the *NcoI-XhoI* restriction sites. Amplification was achieved using specific primer pairs for: $bla_{\text{PDC-3}}$ FF(BamHI) 5’-CCATGGGTCAGGAGGAGGATGCGACG-3’ and $bla_{\text{PDC-3}}$ FR(HindIII) 5’-CTCGAGAAGCCTAGATTTTCCCCGCC-3’; $bla_{\text{PDC-5}}$ FF(BamHI) 5’-CCATGGGCGCTCATGGCACCATCATA-3’ and $bla_{\text{PDC-5}}$ FR(HindIII) 5’-CTCGAGAAGCCTAGATTTTCCCCGCC-3’; $bla_{\text{PDC-10}}$ FF(BamHI) 5’-CCATGGCCAGGTCTTGAGCGACATCC-3’ and $bla_{\text{PDC-10}}$ FR(HindIII) 5’-CTCGAGGAGTATTCGTCGTTTGCCGC-3’; $bla_{\text{PDC-266}}$ FF(BamHI) 5’-CCATGGCACCATCATAGCCAGGACCG-3’ and $bla_{\text{PDC-266}}$ FR(HindIII) 5’-CTCGAGTCTCATGCAGCCAACGACAA-3’; $bla_{\text{OXA-50}}$ FF(BamHI)

5’-CCATGGCTACCCTTTCGTCGCCAAGT-3’ and *bla*$_{\text{OXA-50}}$ FR(HindIII) 5’-CTCGAGTGTATGGCTATCACCTCGGC-3’.The resulting recombinant constructs were introduced into competent *E. coli* DH5α cells via electroporation. Transformants were subsequently propagated in Luria-Bertani broth supplemented with 50 μg/mL kanamycin at 37 °C. Sequence fidelity of all inserted fragments was verified by Sanger sequencing (Personalbio Technology Co., Ltd., Shanghai, China). Pre-cultures grown overnight were diluted 1:100 into fresh medium and incubated under orbital agitation until the optical density at 600 nm reached 0.6–0.8. Protein expression was then induced by adding isopropyl-β-D-thiogalactopyranoside to a final concentration of 1 mM, followed by a 4-hour incubation period. Finally, target proteins were harvested and purified utilizing affinity chromatography with a His-tag Protein Purification Kit.

2.7 Gene Synthesis and Cloning of the Gene of PDC-3-Q79R, PDC-3-N131S, and PDC-3-L205V

To assess how the Q79R, N131S, and L205V substitutions influence the antibiotic and lactase inhibitor susceptibility profiles of PDC-266 relative to the wild-type PDC-3, we constructed three distinct gene variants. Each variant harbored a single specific mutation while retaining the PDC-3 backbone, designated as PDC-3-Q79R, PDC-3-N131S, and PDC-3-L205V, respectively. These genetic sequences were chemically

synthesized and subsequently inserted into the pUCP24 plasmid via a standardized molecular cloning workflow. Target-specific primers were engineered to enable efficient PCR amplification through a two-stage protocol: the initial reaction utilized a 50 μL volume containing 2 μL of both forward and reverse primers, whereas the secondary amplification employed a 100 μL system with doubled reagent concentrations (excluding primers), using the primary product as a template. The resulting amplicons were then integrated into the pUCP24 vector at *HindIII* and *EcoRI* restriction sites utilizing a recombination-based strategy. Following transformation into competent *E. coli* DH5α cells, individual colonies were screened via colony PCR with specific primers to verify insert presence. Putative positive clones underwent further validation through plasmid isolation and double digestion with *HindIII* and *EcoRI*, with final sequence fidelity confirmed by Sanger sequencing (primer sequences are provided in Supplementary Materials).

Parallel procedures were applied to clone the full open reading frames of PDC-3-Q79R, PDC-3-N131S, and PDC-3-L205V into the pET-28a expression vector, targeting the *NcoI* and *XhoI* restriction sites. The recombinant constructs were introduced into competent *E. coli* DH5α cells via calcium chloride-mediated transformation. Transformants were propagated in Luria-Bertani broth supplemented with 50 μg/mL kanamycin at 37 °C, and insert integrity was verified by Sanger

sequencing (Personalbio Technology Co., Ltd., Shanghai, China). Overnight cultures were diluted 100-fold into fresh medium and incubated with orbital agitation until reaching an OD600 of 0.6–0.8. Protein expression was induced by adding isopropyl-β-D-thiogalactopyranoside to a final concentration of 1 mM, followed by a 4-hour incubation period. Recombinant proteins were subsequently purified using affinity chromatography with a His-tag Protein Purification Kit (primer sequences are provided in Supplementary Materials).

2.8 Determination of kinetic parameters

Kinetic constants governing the hydrolysis of β-lactam substrates by purified enzymes (PDC-3, PDC-5, PDC-10, KPC-266, OXA-50, and the PDC-3 variants Q79R, N131S, and L205V) were quantified using ultraviolet-visible spectrophotometry. Assays were conducted at 30 °C in 10 mM phosphate buffer (pH 7.0) within a total reaction volume of 300 μL. Steady-state kinetic parameters (*kcat* and *KM*) were derived by fitting initial velocity data to the Michaelis–Menten model via non-linear regression in GraphPad Prism (version 7; GraphPad Software, San Jose, CA, USA). To assess inhibitory potential, benzylpenicillin (500 μM) served as the reporter substrate. Enzyme preparations underwent a 3-min preincubation at 30 °C with graded concentrations of inhibitors (TZB,

SUL, or AVI) before substrate introduction. The half-maximal inhibitory concentration (IC$_{50}$), defined as the inhibitor dose reducing hydrolysis of 500 μM benzylpenicillin by 50%, was computed through non-linear regression employing the "log(inhibitor) versus response – variable slope" algorithm in Prism.

2.9 Analysis of protein structure and molecular docking

The crystallographic coordinate file for PDC-3(isolated from *P. aeruginosa*, PDB ID: 8SDL) was obtained from RCSB PDB (https://www.rcsb.org/). Leveraging PDC-3 as a structural template, homology models for PDC-266 were constructed using the automated Swiss-Model server (https://swissmodel.expasy.org/). Ligand structures for meropenem (MEM) were acquired in Structure Data File (SDF) format from PubChem (https://pubchem.ncbi.nlm.nih.gov/) and subsequently converted to PDB format utilizing OpenBabel. Prior to docking procedures, crystalline water molecules were excised from protein structures using PyMOL. Docking interactions between each protein target and ligand were simulated with AutoDock Vina, with binding poses ranked according to predicted affinity scores and root-mean-square deviation (RMSD) metrics across conformations.

2.9 Nucleotide accession numbers

The nucleotide sequences reported in this study have been submitted

to the GenBank nucleotide database under the accession number PRJNA1417796, PRJNA1417801, PRJNA1417802 and PRJNA1417812, for PA1CSR, PA2ZBF, PA4WXP and PA6LZZ, respectively.

3. Results

3.1 Distribution of β-lactamase genes and prevalence of *bla*$_{PDC}$s

Five β-lactamase genes were identified and screened for validation after sequencing the genomic DNA of 14 *bla*$_{PDC}$-harboring *P. aeruginosa* strains. Four *bla*$_{PDC}$ variants were identified across the strains: six strains carried *bla*$_{PDC-3}$ (PA2ZBF, PA3AWD, PA5ZXH, PA11TMB, PA12REL, and PA14MSK); five carried *bla*$_{PDC-5}$ (PA6LZZ, PA7DWQ, PA9OGC, PA13HJY, and PA10LPO); two carried *bla*$_{PDC-10}$ (PA4WXP and PA8UHT); and one carried *bla*$_{PDC-266}$ (PA1CSR). Comparing PDC-266 with PDC-3 and PDC-10 reveals three mutation sites: Q79, N131, and L205 in PDC-266 correspond to R79, S131, and V205 in PDC-3 and PDC-10, respectively. In contrast, PDC-266 differs from PDC-5 by only two mutation sites: N131 and L205 in PDC-266 correspond to S131 and V205 in PDC-5, whereas Q79 is identical in both PDC-266 and PDC-5. This implies that the sole difference between PDC-5 and PDC-3/PDC-10 lies at position 79, where PDC-5 has Q79 while PDC-3 and PDC-10 have R79. Furthermore, PDC-3 and PDC-10 differ by only one mutation in their signal peptides (T21 in PDC-3 vs. A21 in PDC-10). However, after

the signal peptide is cleaved, the mature functional protein sequences of PDC-3 and PDC-10 are identical. Therefore, PDC-10 can be considered equivalent to PDC-3. The β-lactamase gene *bla*$_{\text{OXA-50}}$ is the most prevalent gene found in all 14 *bla*$_{\text{PDC}}$-harboring *P. aeruginosa* strains. No other β-lactamase genes were detected in these strains.

3.2 Antimicrobial susceptibility of *bla*$_{\text{PDC}}$ harboring isolates

Minimum inhibitory concentration (MIC) testing of 13 antimicrobials against 14 *bla*$_{\text{PDC}}$-harboring *P. aeruginosa* strains indicated multidrug resistance. All isolates exhibited resistance to various types of β-lactam antimicrobials, thereby displaying a multidrug-resistant (MDR) phenotype. High levels of resistance were observed against aztreonam (AZT), ampicillin (AMP), and ceftriaxone (CTX) with minimum inhibitory concentrations (MICs) exceeding the resistance breakpoints (often >256 μg/mL). Resistance to piperacillin (PIP), piperacillin-tazobactam (TZP), ampicillin/sulbactam (ASP), cefepime (FEP), ceftazidime (CAZ), cefoperazone (CFPM) and cefoperazone/sulbactam (CFPM/SUL), and even the carbapenems (MEM and IMP), was also universal within the clinical isolate cohort. There was almost no difference in MICs of all above antibiotics between different *bla*$_{\text{PDC}}$ harboring isolates, however, the sole *bla*$_{\text{PDC-266}}$ isolate (PA1CSR) demonstrated reduced susceptibility to MEM (64 μg/mL), representing a ≥2-fold increase in MIC (Table 1).

Isolate	CAZ	CAZ/AVI	FEP	MEM	IMP	AZT	ASP	AMP	CFPM/SUL	CFPM	PIP	TZP	CTX	Resistance genes	
PA1CSR	64	4	32	64	16	>256	64	>256	32	64	128	32	>256	*bla*$_{PDC-266}$	*bla*$_{OXA-50}$
PA2ZBF	64	8	32	8	8	>256	64	>256	32	64	64	16	>256	*bla*$_{PDC-3}$	*bla*$_{OXA-50}$
PA3AWD	64	8	32	16	16	>256	32	>256	64	64	64	16	>256	*bla*$_{PDC-3}$	*bla*$_{OXA-50}$
PA4WXP	32	4	16	16	8	>256	64	>256	32	64	128	32	>256	*bla*$_{PDC-10}$	*bla*$_{OXA-50}$
PA5ZXH	64	4	32	16	16	>256	64	>256	32	32	128	32	>256	*bla*$_{PDC-3}$	*bla*$_{OXA-50}$
PA6LZZ	64	4	16	16	16	>256	32	>256	32	32	128	16	>256	*bla*$_{PDC-5}$	*bla*$_{OXA-50}$
PA7DWQ	64	4	32	8	16	>256	32	>256	64	64	64	16	>256	*bla*$_{PDC-5}$	*bla*$_{OXA-50}$
PA8UHT	32	8	32	8	8	>256	64	>256	32	64	128	32	>256	*bla*$_{PDC-10}$	*bla*$_{OXA-50}$
PA9OGC	6	4	1	1	1	>	6	>	3	3	6	1	>	*bla*$_{P}$	*bla*

	4		6	6	6	256>	4	256>	2	2	4	6	256>	DC-5	OXA-50
PA10LPO	32	4	8	8	8	256>	64	256>	32	32	64	8	256>	*bla*PDC-5	OXA-50
PA11TMB	32	8	16	16	16	256>	64	256>	32	64	128	16	256>	*bla*PDC-3	OXA-50
PA12REL	64	8	8	16	8	256>	64	256>	32	64	128	32	256>	*bla*PDC-3	OXA-50
PA13HJY	32	8	16	16	16	256>	64	256>	32	32	128	32	256>	*bla*PDC-5	OXA-50
PA14MSK	64	4	16	8	8	256>	64	256>	32	32	128	16	256>	*bla*PDC-3	OXA-50
DH5α-PDC-266-T	64	2	16	32	4	256>	32	128	8	32	128	16	256>	*bla*PDC-266	
DH5α-PDC-3-T	32	4	16	4	4	256>	32	128	16	32	128	16	256>	*bla*PDC-3	
DH5α-PDC-5-T	32	4	8	2	2	256>	32	128	16	16	128	32	256>	*bla*PDC-3	
DH5α-PDC-10-T	32	4	16	4	4	256>	32	128	16	32	128	16	256>	*bla*PDC-10	
DH5α-PDC-3-Q79R-T	32	4	16	4	4	256>	32	128	16	32	64	16	256>	*bla*PDC-3-Q53R	
DH5α-P	3	2	1	3	4	>	3	1	8	3	1	3	>	*bla*P	

DC-3-N131S-T	2		6	2		256>256	2	32>256		2	32>256	2	256>256	DC-3-N105S	CAZ, ceftazidime; CAZ/AVI ceftazidime/avibactam; FEP, cefepime; MEM, meropenem; IMP, imipenem; AZT, aztreonam; ASP, ampicillin/sulbactam; CTX, ceftriaxone; CFPM/SUL, cefoperazone/sulbactam; TZP, piperacillin-tazobactam; PIP, piperacillin; AMP, ampicillin; CFPM, cefoperazone;
DH5α-PDC-3-L205V-T	32	4	16	4	4	256>256	32	128>256	16	32	64	16	256>256	*bla*PDC-3-L179V	
DH5α-OXA-50-T	32	4	16	32	16	256>256	64	256>256	32	32	128	32	256>256	*bla*OXA-50	
E. coli DH5α	2	0.06 25	2	0.125	0.25	2	4	1	16	128	0.06 25	0.125	0.125		
ATCC 25922	2	0.06 25	2	1	1	2	2	2	0.25	8	0.06 25	0.125	0.125		

Table 1 Antimicrobial susceptibility and β-lactam resistance gene distribution of the 14 *bla*$_{PDC}$-harboring *P. aeruginosa* isolates.

3.3 Transformation assay

Initially, five transformants were constructed to explore the resistant phenotypes of *bla*$_{PDC-3,}$ *bla*$_{PDC-5,}$ *bla*$_{PDC-10,}$ *bla*$_{KPC-266}$ and *bla*$_{OXA-50}$. All five transformants exhibited resistance to CAZ, FEP, AZT, ASP, CTX, TZP, PIP, AMP, CFPM, and CFPM/SUL, with MIC ranges of 32–64, 8–16, >256, 32–64, >256, 16–32, 64–128, 128–>256, 16–32, and 8–16 μg/ml, respectively. All transformants exhibited susceptibility to CAZ/AVI, with an MIC range of 2–4 μg/ml. Transformant DH5α-OXA-50-T exhibited resistance to both MEM and IMP, with MICs of 32 and 16 μg/ml, respectively; this contrasts with transformant DH5α-PDC-266-T, which was resistant to MEM (MIC of 32 μg/ml) but

susceptible to IMP (MIC of 4 μg/ml). Transformants $bla_{PDC-3,}$ bla_{PDC-5} and bla_{PDC-10} were all susceptible to MEM and IMP, with MIC ranges of 2–4 μg/ml.

The antibiotic resistance phenotype of transformant DH5α-PDC-266-T exhibited distinct differences compared to DH5α-PDC-3-T, DH5α-PDC-5-T, and DH5α-PDC-10-T, particularly regarding MEM, with an MIC increased by more than 8-fold. The MIC values for various antibiotics among the three transformants—DH5α-PDC-3-T, DH5α-PDC-5-T, and DH5α-PDC-10-T—did not exhibit significant differences.

Furthermore, to compare the impact of the three mutation sites in PDC-266 relative to PDC-3 on the antibiotic resistance phenotype of *P. aeruginosa*, the genes PDC-3-Q79R, PDC-3-N131S, and PDC-3-L205V were synthesized based on the PDC-3 sequence and subjected to transformation. Compared to DH5α-PDC-3-Q79R-T and DH5α-PDC-3-L205V-T, DH5α-PDC-3-N131S-T demonstrated stronger resistance to MEM, with an MIC increased by more than 8-fold; although transformant DH5α-PDC-3-Q79R-T also exhibited increased resistance to PIP and TZP, with MICs increased by 2-fold.

When comparing transformants containing the synthesized genes to those containing the original genes, the transformant expressing PDC-3-N131S exhibited an antibiotic resistance phenotype similar to

DH5α-PDC-266-T, whereas those expressing PDC-3-Q79R and PDC-3-L205V exhibited phenotypes similar to DH5α-PDC-3-T, DH5α-PDC-5-T, and DH5α-PDC-10-T (Table 1).

3.4 Determination of Kinetic Parameters

Steady-state kinetic analysis was performed to determine the catalytic efficiency of the purified β-lactamases (PDC-26, PDC-3, PDC-5, PDC-10, OXA-50) and the engineered variants (PDC-3-Q79R, PDC-3-N131S, PDC-3-L205V) against a panel of β-lactam antibiotics. Significant variation in substrate specificity was observed among the wild-type enzymes. All the β-lactamases demonstrated high catalytic efficiency against AMP (*K*cat/*Km* range: 1,424 to 2,120 $mM^{-1}\cdot s^{-1}$), PIP (136 to 242 $mM^{-1}\cdot s^{-1}$), CTX (1,900 to 3,080 $mM^{-1}\cdot s^{-1}$) and AZT (3,600 to 4,770 $mM^{-1}\cdot s^{-1}$), In contrast, they showed moderate catalytic efficiency against CAZ (*K*cat/*Km* range: 7.4 to 16 $mM^{-1}\cdot s^{-1}$) and CFPM (7.6 to 17 $mM^{-1}\cdot s^{-1}$), Consequently, all the β-lactamases exhibited low catalytic efficiency against cefepime. PDC-26, OXA-50, and PDC-3-N131S demonstrated moderate catalytic efficiency against MEM, with *K*cat/*Km* 15, 17 and 16.5 $mM^{-1}\cdot s^{-1}$, respectively, whereas the other β-lactamases showed low catalytic efficiency. For imipenem, almost all β-lactamases demonstrated low catalytic efficiency; however, only OXA-50 exhibited moderate catalytic efficiency, with a *K*cat/*Km* 14.6 $mM^{-1}\cdot s^{-1}$(Table 2).

Isolate	CAZ	CAZ/AVI	FEP	MEM	IMP	AZT	ASP	AMP	CFPM/SUL	CFPM	PIP	TZP	CTX	Resistance genes	
PA1CSR	64	4	32	64	16	>256	64	>256	32	64	128	32	>256	*bla*$_{PDC-266}$	*bla*$_{OXA-50}$
PA2ZBF	64	8	32	8	8	>256	64	>256	32	64	64	16	>256	*bla*$_{PDC-3}$	*bla*$_{OXA-50}$
PA3AWD	64	8	32	16	16	>256	32	>256	64	64	64	16	>256	*bla*$_{PDC-3}$	*bla*$_{OXA-50}$
PA4WXP	32	4	16	16	8	>256	64	>256	32	64	128	32	>256	*bla*$_{PDC-10}$	*bla*$_{OXA-50}$
PA5ZXH	64	4	32	16	16	>256	64	>256	32	32	128	32	>256	*bla*$_{PDC-3}$	*bla*$_{OXA-50}$
PA6LZZ	64	4	16	16	16	>256	32	>256	32	32	128	16	>256	*bla*$_{PDC-5}$	*bla*$_{OXA-50}$
PA7DWQ	64	4	32	8	16	>256	32	>256	64	64	64	16	>256	*bla*$_{PDC-5}$	*bla*$_{OXA-50}$
PA8UHT	32	8	32	8	8	>256	64	>256	32	64	128	32	>256	*bla*$_{PDC-10}$	*bla*$_{OXA-50}$
PA9OGC	6	4	1	1	1	>	6	>	3	3	6	1	>	*bla*$_{P}$	*bla*

	4		6	6	6	256>	4	256>	2	2	4	6	256>	DC-5	OXA-50
PA10LPO	32	4	8	8	8	256>	64	256>	32	32	64	8	256>	*bla*PDC-5	OXA-50
PA11TMB	32	8	16	16	16	256>	64	256>	32	64	128	16	256>	*bla*PDC-3	OXA-50
PA12REL	64	8	8	16	8	256>	64	256>	32	64	128	32	256>	*bla*PDC-3	OXA-50
PA13HJY	32	8	16	16	16	256>	64	256>	32	32	128	32	256>	*bla*PDC-5	OXA-50
PA14MSK	64	4	16	8	8	256>	64	256>	32	32	128	16	256>	*bla*PDC-3	OXA-50
DH5α-PDC-266-T	64	2	16	32	4	256>	32	128	8	32	128	16	256>	*bla*PDC-266	
DH5α-PDC-3-T	32	4	16	4	4	256>	32	128	16	32	128	16	256>	*bla*PDC-3	
DH5α-PDC-5-T	32	4	8	2	2	256>	32	128	16	16	128	32	256>	*bla*PDC-3	
DH5α-PDC-10-T	32	4	16	4	4	256>	32	128	16	32	128	16	256>	*bla*PDC-10	
DH5α-PDC-3-Q79R-T	32	4	16	4	4	256>	32	128	16	32	64	16	256>	*bla*PDC-3-Q53R	
DH5α-P	3	2	1	3	4	>	3	1	8	3	1	3	>	*bla*P	

DC-3-N131S-T	2		6	2		256	2	8		2	28	2	256	DC-3-N105S		
DH5α-PDC-3-L205V-T	32	4	16	4	4	>256	32	128	16	32	64	16	>256	*bla*PDC-3-L179V		
DH5α-OXA-50-T	32	4	16	32	16	>256	64	>256	32	32	128	32	>256	*bla*OXA-50		
E. coli DH5α	2	0.0625	2	0.125	0.25	2	4	1	16	128	0.0625	0.125	0.125			
ATCC 25922	2	0.0625	2	1	1	2	2	2	0.25	8	0.0625	0.125	0.125			

CAZ, ceftazidime; CAZ/AVI ceftazidime/avibactam; FEP, cefepime; MEM, meropenem; IMP, imipenem; AZT, aztreonam; ASP, ampicillin/sulbactam; CTX, ceftriaxone; CFPM/SUL, cefoperazone/sulbactam; TZP, piperacillin-tazobactam; PIP, piperacillin; AMP, ampicillin; CFPM, cefoperazone

Table 1 Antimicrobial susceptibility and β-lactam resistance gene distribution of the 14 *bla*$_{PDC}$-harboring *P. aeruginosa* isolates.

The IC50 values (50% inhibitory concentrations) determined for β-lactamase inhibition assays indicated that avibactam (with IC50 values ranging from 17.2 ± 3.3 to 20.8 ± 4.2 nM) and sulbactam (with IC50 values ranging from 19.4 ± 4.0 to 26.7 ± 6.3 nM) demonstrated higher inhibitory efficiency against variant PDCs compared to tazobactam (with IC50 values ranging from 99.3 ± 16.2 to 184.3 ± 20.2 nM) (Table 3). When comparing the inhibition efficiencies of the respective inhibitors across the PDC variants, all transformants exhibited similar inhibitory susceptibility. For OXA-50, avibactam demonstrated higher inhibitory efficiency compared to sulbactam and tazobactam.

Table 3 Inhibition kinetics with wild-type and synthesized β-lactamases

Inhibitor	PDC-266	PDC-3	PDC-5	PDC-10	OXA-50	PDC-3-Q53R	PDC-3-N105S	PDC-3-L179V
Avibactam	18.2 ± 4.7	18.8 ± 5.0	17.2 ± 3.3	18.2 ± 4.4	27.8 ± 5.8	19.5 ± 5.6	18.0 ± 4.2	20.8 ± 4.2
Sulbactam	20.9 ± 4.4	22.2 ± 3.6	24.0 ± 4.9	25.6 ± 6.2	193.1 ± 26.6	24.8 ± 5.7	19.4 ± 4.0	26.7 ± 6.3
Tazobactam	104.5 ± 23.6	184.3 ± 20.2	173.3 ±18.9	180.3 ± 15.2	222.3 ± 20.2	178.6 ± 18.4	99.3 ± 16.2	182.5 ± 25.7

Affinity percent inhibitory concentration (IC50: nM) values were determined spectrophotometrically following a 5-min preincubation of inhibitor and enzyme, corrected for competition of the reporter substrate, and are provided in nanomolar as the mean±standard deviation of three independent replicates.

3.5 PFGE typing and MLST

We used PFGE to type 14 *bla*$_{PDC}$-positive strains carrying one *bla*$_{PDC-266}$, two *bla*$_{PDC-10}$, five *bla*$_{PDC-5}$ and six *bla*$_{PDC-3}$ alleles to determine their prevalence. Each isolate was typeable and clustered into six clusters, namely A to F (Figure 1). The predominant clusters, A, B and D contained six,two and three of all 14 strains (n = 6/14, 2/14 and 3/14, respectively), whereas the other three clusters (C, E and F) contained only one strain each. MLST analysis divided the 14 *bla*$_{PDC}$-harboring strains into two different sequence types (STs) (7 strains of ST235, and other 7 strains of ST244) (Figure 1). Strains belonging to ST235 corresponded to PFGE pulsotypes A and D (both n = 2) and B, C, and E (all n = 1), whereas ST244 corresponded to PFGE pulsotypes A (n = 4), B (n = 1), D (n = 1), and F (n = 1), respectively. The *bla*$_{PDC}$-266-positive strain corresponded to PFGE pulsotype F.

3.6 Comparative genomic analysis of *bla*$_{PDC}$ related regions

The whole-genome sequences of four isolates (PA1CSR, PA3AWD, PA4WXP and PA6LZZ) were acquired. All the sequences harbored two types of β-lactamases-*bla*$_{PDC}$ and *bla*$_{OXA,}$ while *bla*$_{OXA-50}$ was the unique *bla*$_{OXA}$ type in the four chromosome sequences, the *bla*$_{PDC}$ types were diverse, including *bla*$_{PDC-266}$ in PA1CSR, *bla*$_{PDC-3}$ in PA3AWD, *bla*$_{PDC-10}$

in PA4WXP and *bla*$_{PDC-5}$ in PA6LZZ. The four sequences also harbored similar types of antibiotic resistance enzyme genes such as glycopeptide resistance enzymes (vanW and vanH) and aminoglycoside-modifying enzymes (APH(3')-IIb). The *bla*$_{PDC}$ gene is located in close proximity to APH(3')-IIb, whereas the distance to *bla*$_{OXA-50}$ is approximately 1 Mb. As a member of the AmpC enzymes, *bla*$_{PDC}$ is closely linked to the AmpC enzyme regulatory protein AmpR with the intercistronic region containing the promoter of each genes. Based on the antibiotic resistance genes identified in the sequences of these Pseudomonas aeruginosa strains, it is evident that the MexA/B-OprM efflux pump system is also one of the primary contributors to multidrug resistance (MDR) in this bacterium (Figure 2).

3.7 Molecule docking analysis

The crystal structures of PDC-3 and PDC-266 are similar. Although the positions of the binding cavities have not changed, the shape of the cavities has undergone certain alterations. Specifically, the largest cavity in PDC-3 is characterized by a volume of 408.75 Å^3, a maximum surface area of 391.33 Å^2, an average depth of 2.41 Å, and a maximum depth of 7.61 Å. In contrast, the corresponding cavity in PDC-266 has a volume of 355.1 Å^3, a maximum surface area of 329.34 Å^2, an average cavity depth of 2.97 Å, and a maximum depth of 9.6 Å. Relative to PDC-3, the cavity in PDC-266 is narrower and deeper (Figure 3).

In the structures of both PDC-3 and PDC-266, the ligand meropenem is located within the largest cavity. In PDC-3, meropenem is positioned closer to the deep-cavity residue SER-131, whereas in PDC-266, it is closer to residue SER-64 than to the N131S variant of SER-131.

In the PDC-3 structure, meropenem forms 5 hydrogen bonds: the N and O atoms on the bicyclic nitrogen-oxygen system form 2 hydrogen bonds with the Oγ atom of SER-131; the O atom on the nitrogen-oxygen bicycle forms one hydrogen bond with the Hγ atom of LEU-133; and the O atoms on the carboxyl group form one hydrogen bond each with the Oγ atoms of ASN-134 and THR-139 (Figure 4).

In the PDC-266 structure, meropenem forms 8 hydrogen bonds: the carboxyl group of meropenem forms one hydrogen bond with SER-64; the N and O atoms on the nitrogen-oxygen bicycle form 2 hydrogen bonds with the Oγ atom of ALA-136; the O atom on the nitrogen-oxygen bicycle and the carbonyl O atom on the pyrrolidine ring side chain form one hydrogen bond each with the backbone N atom of GLY-297; the O atom on the nitrogen-oxygen bicycle and the carbonyl H atom on the pyrrolidine ring side chain form one hydrogen bond each with the side chain Hγ atom of GLY-295; and the carbonyl O atom on the pyrrolidine ring side chain forms another hydrogen bond with the Hγ atom of GLN-294 (Figure 5).

4. Discussion

The global epidemiology of PDCs indicates that certain variants are more prevalent than others. Specifically, PDC-3, PDC-5, and PDC-17 have emerged as dominant circulating enzymes in clinical isolates(11). The evolution of these enzymes is driven by point mutations that alter the enzyme's active site or regulatory regions. Notably, amino acid substitutions such as Val211Gly and Asp213Gly are frequently observed in extended-spectrum AmpC (ESAC) variants. These specific mutations are often associated with an expanded hydrolytic spectrum, enabling the enzyme to confer resistance to third-generation cephalosporins, including ceftazidime and cefepime, thereby complicating treatment regimens for severe pseudomonal infections(12,13). This study investigated the molecular epidemiology, genetic context, and biochemical characteristics of PDC variants, with a particular focus on the variant PDC-266 identified in clinical isolates. and characterized its genetic context, hydrolytic profile, and structural determinants of antibiotic resistance. Our findings expand the understanding of allelic diversity within the PDC family and highlight how discrete amino acid substitutions can modulate substrate specificity and resistance phenotypes.

The distribution of *bla*$_{\text{PDC}}$ genes among the 14 clinical isolates revealed a predominance of *bla*$_{\text{PDC-3}}$ and *bla*$_{\text{PDC-5}}$, with a single isolate

harboring the novel variant *bla*$_{\text{PDC-266}}$. Sequence alignment showed that PDC-266 differs from PDC-3 and PDC-10 at three residues (Q79R, N131S, L205V) and from PDC-5 at two residues (N131S, L205V). Alterations in the PDC Ω-loop, associated with resistance to newer β-lactam/inhibitor combinations, were common in P. aeruginosa clinical isolates; notably, the amino acid substitution Y221H in the Ω-loop of Pseudomonas-derived cephalosporinase (PDC) confers resistance to the critical anti-pseudomonal antibiotics ceftazidime and ceftolozane. A key study found that the E221K variant, which emerged under selective pressure, confers the most significant resistance, increasing the MIC of ceftolozane by 128-fold and ceftazidime by 32-fold compared to the wild-type enzyme. Kinetic analyses confirmed a dramatic increase in catalytic efficiency (kcat/Km) for ceftazidime hydrolysis by the E221K variant(14). Although V205L is found frequently in the Ω-loop of various variants such as PDC-35, PDC-39, PDC-90, PDC-91, and PDC-92, an association with resistance has not been demonstrated(15,16,17). The specific mutation R79Q in the PDC enzyme was also commonly observed in PDC variants, with the R79Q amino acid substitution near the H-2 helix. A study found that these PDC types were exclusively present in the MEM > MEV group, but it did not confirm an association between the R79Q mutation and MEM resistance(18). Unfortunately, the mutation N131S is rarely reported in the literature. The presence of *bla*$_{\text{OXA-50}}$ in all

14 strains is consistent with its role as a conserved chromosomal β-lactamase in P. aeruginosa, further supporting the intrinsic resistance background of this species(19).

Antimicrobial susceptibility testing demonstrated that all *bla*$_{PDC}$-harboring isolates exhibited multidrug resistance, characterized by elevated MICs for penicillins, cephalosporins, and aztreonam. Notably, the PDC-266-producing isolate PA1CSR exhibited elevated MICs for meropenem (64 μg/mL) relative to strains harboring other PDC variants. This observation suggests that specific mutations in PDC-266 may confer subtle but clinically relevant carbapenem hydrolytic activity, a feature not typically associated with wild-type PDCs(20). Resistance to piperacillin-tazobactam and ceftazidime-avibactam in a subset of isolates highlights the limitations of β-lactam/β-lactamase inhibitor combinations in the context of evolving PDC variants(21).

Transformation assays provided direct evidence that the resistance phenotype of PDC-266 is primarily conferred by the *bla*$_{PDC-266}$ gene itself. Transformants expressing PDC-266 showed significantly higher MICs for meropenem compared to those expressing PDC-3, PDC-5, or PDC-10. Among the single-site mutants, the N131S substitution alone recapitulated the meropenem resistance phenotype, implicating this residue as a key determinant of expanded substrate specificity. This finding indicates single residue mutation in helix can alter the active site

architecture and enable hydrolysis of bulky substrates(22,23). Kinetic analysis further corroborated these observations. PDC-266 and the PDC-3-N131S variant exhibited measurable catalytic efficiency against meropenem ((*K*cat/*Km* range: 15 to 16.5 $mM^{-1} \cdot s^{-1}$), whereas other PDC variants showed negligible activity. This represents a rare instance of acquired carbapenemase-like activity in a PDC enzyme(24). In this study, transformant of R79Q amino acid substitution didn't present any change of the resistance phenotype compared to PDC-3, although the previous reseach revealed the occurrence R79Q related to antibiotics' pressure(25). Similarly, L205V substitution also didn't present any change of the resistance phenotype compared to PDC-3, although this position located in Ω-loop, indicate the mutation is neutral substitution, differ to Val211Gly and Asp213Gly(26).

Molecular docking analysis revealed structural basis for the altered substrate profile. The active site cavity of PDC-266 is narrower and deeper than that of PDC-3, resulting in a repositioning of meropenem toward residues such as SER-64 (the catalytic site) and GLY-295 located within the R2 loop, rather than toward SER-131. The formation of additional hydrogen bonds in the PDC-266–meropenem complex likely enhances substrate stabilization and facilitates hydrolysis(27). These structural changes, driven by the N131S substitution, appear to remodel the binding pocket to accommodate carbapenems, a phenomenon

previously described in other AmpC variants, suggesting increased active-site flexibility that may facilitate substrate accommodation and catalysis. Many substitutions (such as M182T in TEM) do not directly alter the interaction between enzymes and antibiotics, but rather compensate for the negative effects of mutations that can expand the resistance spectrum but damage the enzyme structure by enhancing the overall stability of the enzyme(28). This "global inhibition" mechanism enables bacteria to accumulate multiple drug-resistant mutations without losing function, explaining the emergence of complex drug-resistant phenotypes such as those resistant to broad-spectrum cephalosporins and enzyme inhibitors(29,30,31). So despite of the distances of positions R79Q and V205L are far away from SER-64 and N131S, the influence of substitution needed further research(32).

PFGE and MLST analyses indicated that the *bla*$_{\text{PDC}}$ -harboring isolates belonged to two major sequence types, ST235 and ST244, which are globally disseminated high-risk clones associated with multidrug resistance(33). The PDC-266-producing strain PA1CSR was assigned to a unique PFGE pulsotype (F) and ST244, suggesting that this variant may have emerged independently rather than through clonal expansion, potentially facilitated by local antimicrobial selection pressures rather than a single outbreak event.

5. Conclusion

This study characterizes a particular β-lactamase variant, PDC-266, in Pseudomonas aeruginosa, which exhibits an expanded hydrolysis spectrum, including activity against meropenem. The N131S substitution is identified as the critical determinant of this phenotypic shift. PDC-266 remains susceptible to avibactam and sulbactam, offering potential therapeutic options. Genomic and epidemiological analyses place this variant within globally disseminated high-risk clones, underscoring the clinical relevance of ongoing PDC evolution. These findings emphasize the importance of molecular surveillance and structural analysis in anticipating and addressing emerging resistance mechanisms.

6. Conflict of Interest

The authors declare that the research was conducted in the absence of any commercial or financial relationships that could be construed as a potential conflict of interest.

7. Author Contributions

Hailong Lin: Writing – review & editing, Writing – original draft, Visualization, Software, Project administration, Methodology, Investigation, Formal analysis, Conceptualization. **Jian Zhou**: Writing – review & editing, Project administration, Methodology, Formal analysis, Conceptualization. **Leting Huang**: Writing – original draft, Methodology,

Data curation, Investigation. **Kaichun Lin**: Writing – review & editing, Validation, Formal analysis. **Pan Lv**: Writing – review & editing, Resources, Supervision, Methodology, Funding acquisition. All authors have read and consented to the published version of the manuscript.

8. Funding

This work was supported by Jinhua Municipal Science and Technology Bureau， Zhejiang Province (CN, no. 2024-4-313).

9. Acknowledgments

The authors would like to thank the participants, who made this study possible.

10. Ethics approval and consent to participate

This study was conducted in accordance with the ethical principles outlined in the Declaration of Helsinki. The protocol was reviewed and approved by the First People's Hospital of Yongkang’s Institutional Ethics Committee (approval number: YKSDYRMYYEC2024-LW-KS-005). Written informed consent was obtained from all participants prior to their enrollment in the study. Participants were informed of their right to withdraw from the study at any time without consequences. All data were anonymized to protect participant confidentiality.

11. Data Availability Statement

The microbiome data associated with this study have been deposited

in the NCBI GenBank nucleotide database under the accession number PRJNA1417796, PRJNA1417801, PRJNA1417802 and PRJNA1417812, for PA1CSR, PA2ZBF, PA4WXP and PA6LZZ, respectively.

12. Consent for publication

Not Applicable.

References

1. Juan C, Peña C, Oliver A. Host and Pathogen Biomarkers for Severe Pseudomonas aeruginosa Infections. J Infect Dis. 2017;215(suppl_1):S44-S51. doi:10.1093/infdis/jiw299.
2. Ruedas-López A, Alonso-García I, Lasarte-Monterrubio C, et al. Selection of AmpC β-Lactamase Variants and Metallo-β-Lactamases Leading to Ceftolozane/Tazobactam and Ceftazidime/Avibactam Resistance during Treatment of MDR/XDR Pseudomonas aeruginosa Infections. Antimicrob Agents Chemother. 2022;66(2):e0206721. doi:10.1128/AAC.02067-21.
3. Antonelli A, D'Andrea MM, Vaggelli G, Docquier JD, Rossolini GM. OXA-372, a novel carbapenem-hydrolysing class D β-lactamase from a Citrobacter freundii isolated from a hospital wastewater plant. J Antimicrob Chemother. 2015;70(10):2749-2756. doi:10.1093/jac/dkv181.
4. Roberts MG, Burgess S, Toombs-Ruane LJ, Benschop J, Marshall JC, French NP. Combining mutation and horizontal gene transfer in a within-host model of antibiotic resistance. Math Biosci. 2021; 339:108656. doi:10.1016/j.mbs.2021.108656.
5. Singh A, Turner JM, Tomberg J, et al. Mutations in penicillin-binding protein 2 from cephalosporin-resistant *Neisseria gonorrhoe*a hinder ceftriaxone acylation by restricting protein dynamics. J Biol Chem. 2020;295(21):7529-7543. doi:10.1074/jbc.RA120.012617.
6. Karthik M, Kacha S, Rajendran S, et al. Genetic characteristics and diversity of PDC variants of Pseudomonas aeruginosa and its clinical relevance. Infect Genet Evol. 2024;126:105701. doi:10.1016/j.meegid.2024.105701.
7. Gaibani P, Amadesi S, Lazzarotto T, Ambretti S. Complete Genome Sequence of a Multidrug-Resistant *Klebsiella pneumoniae* Strain Carrying bla_{OXA181} and $bla_{\text{KPC-125}}$ Carbapenemase. Microb Drug Resist. 2022;28(9):916-920. doi:10.1089/mdr.2022.0143.
8. Haidar G, Clancy CJ, Shields RK, Hao B, Cheng S, Nguyen MH. Mutations in $bla_{\text{KPC-3}}$ That Confer Ceftazidime-Avibactam Resistance Encode Novel KPC-3 Variants That Function as Extended-Spectrum β-Lactamases. Antimicrob Agents

Chemother. 2017;61(5). doi:10.1128/AAC.02534-16.
9. Brun T, Péduzzi J, Caniça MM, et al. Characterization and amino acid sequence of IRT-4, a novel TEM-type enzyme with a decreased susceptibility to beta-lactamase inhibitors. FEMS Microbiol Lett. 1994;120(1-2):111-7. doi:10.1111/j.1574-6968.1994.tb07016.x.
10. Ripoll A, Baquero F, Novais A, et al. In vitro selection of variants resistant to beta-lactams plus beta-lactamase inhibitors in CTX-M beta-lactamases: predicting the in vivo scenario? Antimicrob Agents Chemother. 2011;55(10):4530-6. doi:10.1128/AAC.00178-11.
11. de Almeida VF, Urzêdo JE, Velikkakam T, et al. Effector genes of type III secretion system and biofilm formation in virulent *Pseudomonas aeruginosa* isolates carrying $bla_{\text{KPC-2}}$ and $bla_{\text{PDC-5}}$ genes in hospital environment. J Med Microbiol. 2025;74(1). doi:10.1099/jmm.0.001956.
12. Mack AR, Kumar V, Taracila MA, et al. Natural protein in the Ω-loop: the role of Y221 in ceftazidime and ceftolozane resistance in *Pseudomonas*-derived cephalosporinase. Antimicrob Agents Chemother. 2023;67(11):e0079123. doi:10.1128/aac.00791-23.
13. Philippon A, Arlet G, Labia R, Iorga BI. Class C β-Lactamases: Molecular Characteristics. Clin Microbiol Rev. 2022;35(3):e0015021. doi:10.1128/cmr.00150-21.
14. Barnes MD, Taracila MA, Rutter JD, et al. Deciphering the Evolution of Cephalosporin Resistance to Ceftolozane-Tazobactam in *Pseudomonas aeruginosa*. mBio. 2018;9(6):e02085-18. doi:10.1128/mBio.02085-18.
15. Park IS, Walsh CT. D-Alanyl-D-lactate and D-alanyl-D-alanine synthesis by D-alanyl-D-alanine ligase from vancomycin-resistant *Leuconostoc mesenteroides*. Effects of a phenylalanine 261 to tyrosine mutation. J Biol Chem. 1997;272(14):9210-9214. doi:10.1074/jbc.272.14.9210.
16. Park IS, Lin CH, Walsh CT. Gain of D-alanyl-D-lactate or D-lactyl-D-alanine synthetase activities in three active-site mutants of the *Escherichia coli* D-alanyl-D-alanine ligase B. Biochemistry. 1996;35(32):10464-10471. doi:10.1021/bi9603128.
17. Haruta S, Nukaga M, Sawai T. Characterization of an extended-spectrum class C beta-lactamase of *Citrobacter freundii*. Microbiol Immunol. 2001;45(4):277-283. doi:10.1111/j.1348-0421.2001.tb02619.x.
18. Wang YJ, Tayo BO, Bandyopadhyay A, et al. The association of the vanin-1 N131S variant with blood pressure is mediated by endoplasmic reticulum-associated degradation and loss of function. PLoS Genet. 2014;10(9):e1004641. doi:10.1371/journal.pgen.1004641.
19. Alshammari HO, Albarrag AM, Moussa IM, Al-Tawfiq JA, Aldakeel SA, Somily AM. Molecular analysis of carbapenemase-producing Pseudomonas aeruginosa strains in a tertiary care hospital in Riyadh. J Infect Public Health. 2026;19(4):103159. doi:10.1016/j.jiph.2026.103159.
20. Jahan MI, Rahaman MM, Hossain MA, Sultana M. Occurrence of intI1-associated VIM-5 carbapenemase and co-existence of all four classes of β-lactamase in

carbapenem-resistant clinical Pseudomonas aeruginosa DMC-27b. J Antimicrob Chemother. 2020;75(1):86-91. doi:10.1093/jac/dkz426.
21. Arca-Suárez J, Vázquez-Ucha JC, Fraile-Ribot PA, et al. Molecular and biochemical insights into the in vivo evolution of AmpC-mediated resistance to ceftolozane/tazobactam during treatment of an MDR Pseudomonas aeruginosa infection. J Antimicrob Chemother. 2020;75(11):3209-3217. doi:10.1093/jac/dkaa291.
22. Ali A, Azam MW, Khan AU. Non-active site mutation (Q123A) in New Delhi metallo-β-lactamase (NDM-1) enhanced its enzyme activity. Int J Biol Macromol. 2018; 112:1272-1277. doi:10.1016/j.ijbiomac.2018.02.091.
23. Yang WZ, Ko TP, Corselli L, Johnson RC, Yuan HS. Conversion of a beta-strand to an alpha-helix induced by a single-site mutation observed in the crystal structure of Fis mutant Pro26Ala. Protein Sci. 1998;7(9):1875-1883. doi:10.1002/pro.5560070904.
24. Bae DW, Jung YE, Jeong BG, Cha SS. Novel inhibition mechanism of carbapenems on the ACC-1 class C β-lactamase. Arch Biochem Biophys. 2020;693:108570. doi:10.1016/j.abb.2020.108570.
25. Castanheira M, Doyle TB, Hubler CM, DeVries S, Shortridge D. Vaborbactam increases meropenem susceptibility in Pseudomonas aeruginosa clinical isolates displaying MexXY and AmpC upregulation. mSphere. 2023;8(5):e0016223. doi: 10.1128/msphere.00162-23.
26. Barnes MD, Taracila MA, Rutter JD, et al. Deciphering the Evolution of Cephalosporin Resistance to Ceftolozane-Tazobactam in Pseudomonas aeruginosa. mBio. 2018;9(6):e02085-18. doi:10.1128/mBio.02085-18.
27. Gutiérrez S, Correa A, Hernández-Gómez C, De La Cadena E, Pallares C, Villegas MV. Detection of carbapenemase-producing Pseudomonas aeruginosa: Evaluation of the carbapenem inactivation method (CIM). Enferm Infecc Microbiol Clin (Engl Ed). 2019;37(10):648-651. doi:10.1016/j.eimc.2019.02.004.
28. Jacquier H, Birgy A, Le Nagard H, et al. Capturing the mutational landscape of the beta-lactamase TEM-1. Proc Natl Acad Sci U S A. 2013;110(32):13067-13072. doi:10.1073/pnas.1215206110.
29. Bonomo RA, Rice LB. Inhibitor resistant class A beta-lactamases. Front Biosci. 1999; 4:e34-41. doi:10.2741/A477.
30. Cantón R, Morosini MI, de la Maza OM, de la Pedrosa EG. IRT and CMT beta-lactamases and inhibitor resistance. Clin Microbiol Infect. 2007;14,Suppl 1:53-62. doi:10.1111/j.1469-0691.2007.01849.x.
31. Vakulenko S, Golemi D. Mutant TEM beta-lactamase producing resistance to ceftazidime, ampicillins, and beta-lactamase inhibitors. Antimicrob Agents Chemother. 2002;46(3):646-653. doi:10.1128/AAC.46.3.646-653.2002.
32. Shi Y, Rhodes NR, Abdolvahabi A, et al. Deamidation of asparagine to aspartate destabilizes Cu, Zn superoxide dismutase, accelerates fibrillization, and mirrors ALS-linked mutations. J Am Chem Soc. 2013;135(42):15897-15908. doi:10.1021/ja407801x.
33. Slekovec C, Robert J, van der Mee-Marquet N, et al. Molecular epidemiology of Pseudomonas aeruginosa isolated from infected ICU patients: a French multicenter

2012-2013 study. Eur J Clin Microbiol Infect Dis. 2019;38(5):921-926. doi:10.1007/s10096-019-03519-w.

Figure legends

Figure 1. Pulsed-field gel electrophoresis patterns of 14 *bla*$_{PDC}$-positive *P. aeruginosa*.

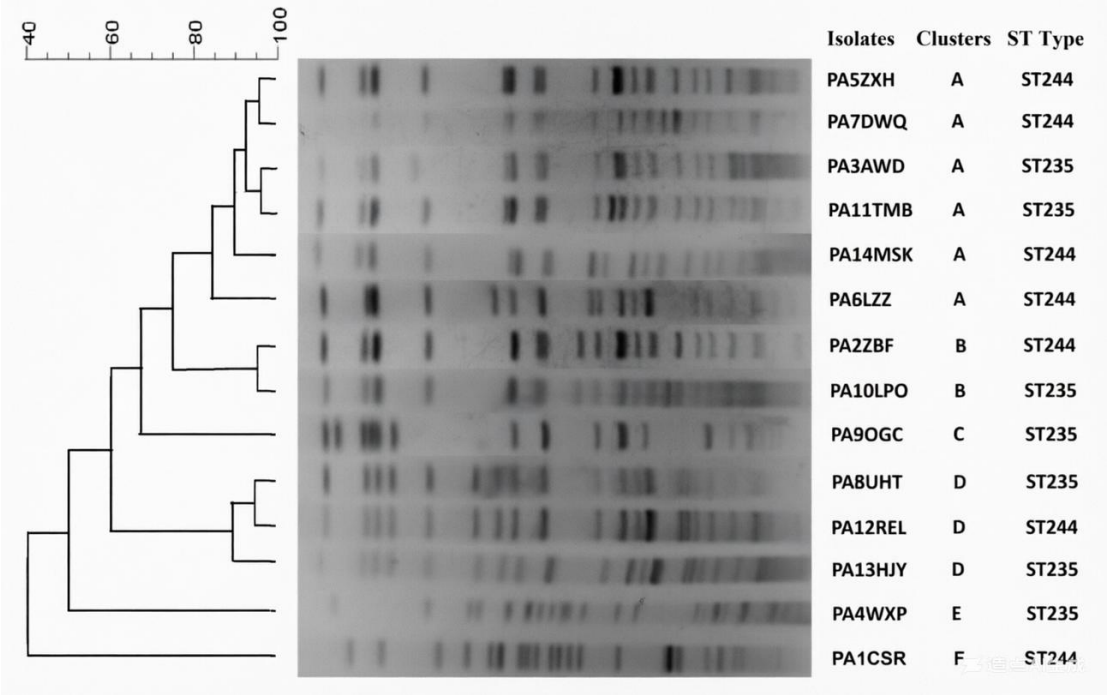
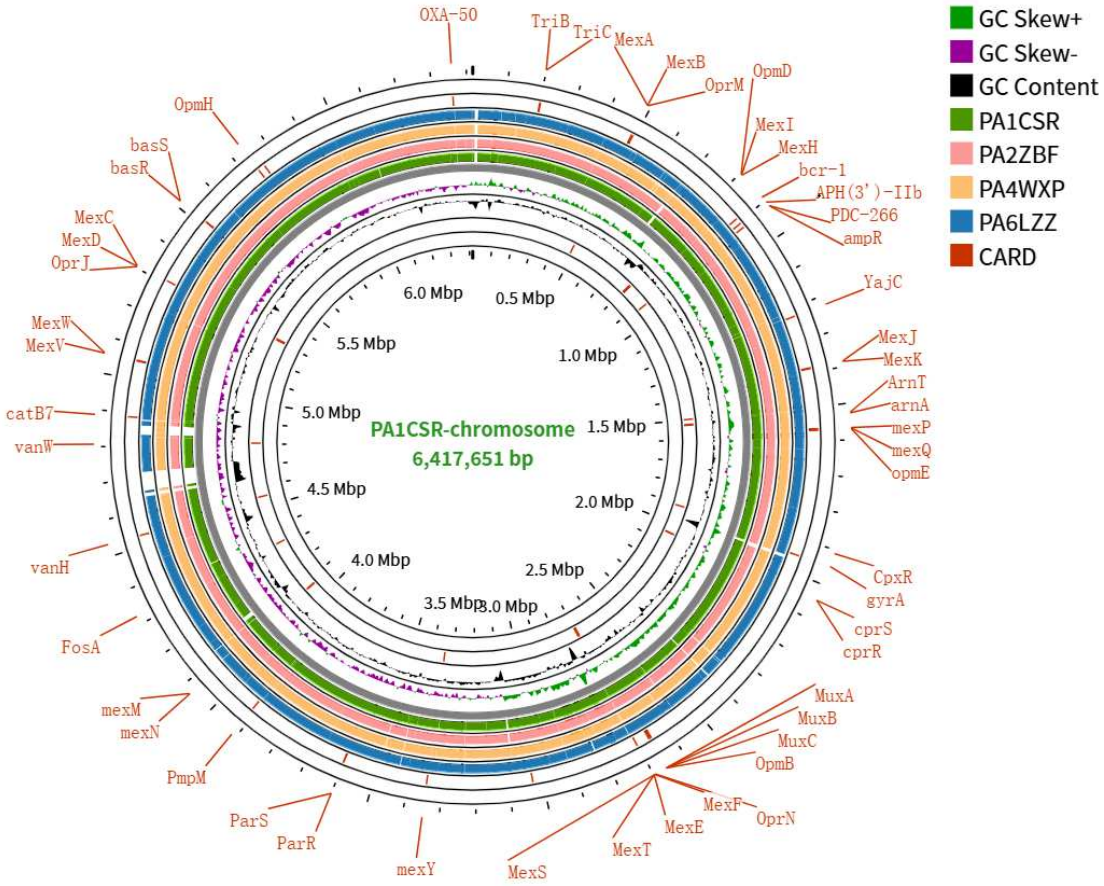


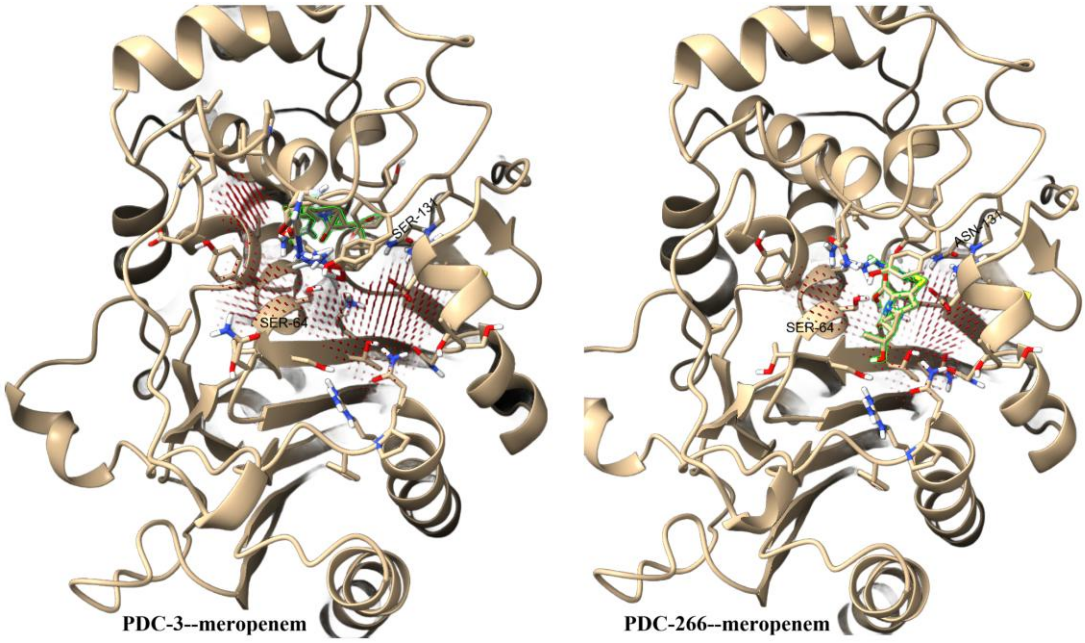
Figure 2. Comparative genomic analysis of the Pseudomonas aeruginosa PA1CSR chromosome



The circular genome map illustrates the 6,417,651 bp chromosome of Pseudomonas aeruginosa PA1CSR, visualized using a comparative genomics approach. From the outermost to the innermost ring: 1. Genomic features and resistance determinants: Annotation tracks highlight key antibiotic resistance genes, efflux pump components, and regulatory elements. 2. GC skew (+) (green): Indicates the deviation of guanine (G) over cytosine (C) on the forward strand. 3. GC skew (−) (purple): Indicates the deviation of cytosine (C) over guanine (G) on the reverse strand. 4. GC content (black): Plotted as deviation from the average genomic GC content. 5Comparative alignment tracks (color-coded): PA1CSR (green); PA2ZBF (pink); PA4WXP (orange);

PA6LZZ (blue). 5.CARD (red): Annotation of antibiotic resistance genes based on the Comprehensive Antibiotic Resistance Database (CARD).

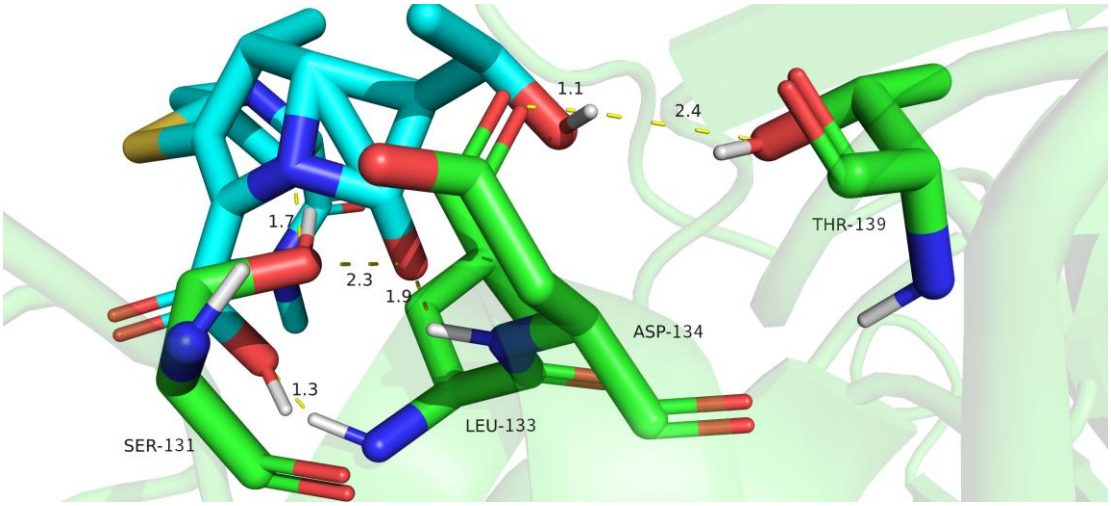
Figure 3. Structural characterization of the PDC-3 and PDC-266 β-lactamases and their interaction with meropenem



(A) Ribbon representation of the PDC-3 protein structure. (B) Ribbon representation of the PDC-266 protein structure. The catalytic serine residues, SER-64 and SER-131 of PDC-3, SER-64 and ASN-131 of PDC-266, are highlighted. The red dashed mesh indicates the cross-sectional area of the active site pocket entrance. The green fluorescent label represents the bound meropenem ligand within the catalytic cavity.

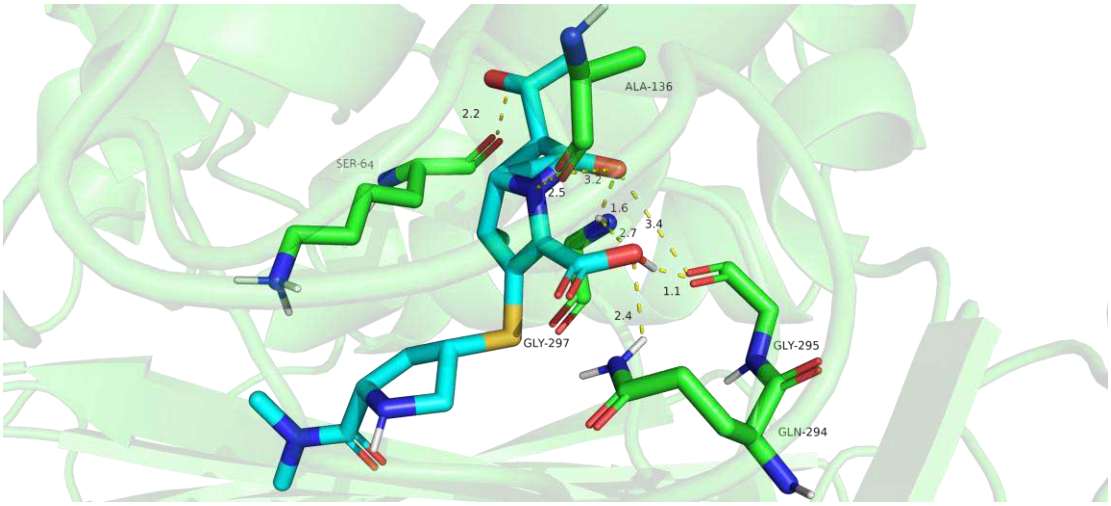
Figure 4. Molecular docking simulation of meropenem (cyan

sticks) within the active site of PDC-3.



The protein backbone is depicted as a light green ribbon, while key interacting residues—Ser131, Leu133, Asp134, and Thr139—are rendered as green sticks. Yellow dashed lines indicate hydrogen bonding interactions between the ligand and the enzyme, with specific interatomic distances annotated in Ångströms (Å). Notably, the β-lactam carbonyl oxygen of meropenem forms a hydrogen bond with the backbone amide of Ser131 (1.7 Å) and the side chain of Thr139 (2.4 Å), while the carboxylate group interacts with Leu133 (1.3 Å) and Asp134 (1.9 Å).

Figure 5. Molecular docking simulation of meropenem (cyan sticks) within the active site of PDC-266.



The PDC-266 protein is shown as a light green ribbon diagram, with key amino acid residues (SER-64, ALA-136, GLN-294, GLY-295, and GLY-297) represented as green sticks. The meropenem molecule is depicted in a cyan stick representation. Yellow dashed lines illustrate the predicted hydrogen bonds between meropenem and the enzyme's active site, with corresponding interatomic distances labeled in angstroms (Å). Notable interactions include hydrogen bonds with the side chains of SER-64 (2.2 Å) and GLN-294 (1.1 Å and 2.4 Å), as well as the backbone atoms of GLY-295 (3.4 Å) and GLY-297 (1.6 Å and 2.7 Å).

Supplementary Files

This is a list of supplementary files associated with this preprint. Click to download.

- Table1.docx
- Table2.docx
- Table3.docx
- supplementaryfilesprimersmix.xlsx
- supplementaryforFigure1PFGEOrigin.tif